Sphere Drag at Transonic Speeds and High Reynolds Numbers

A. B. Bailey* and R. F. Starr†
ARO, Arnold Air Force Station, Tenn.

MEASUREMENTS of sphere drag have been made in the AEDC aeroballistics range "G" over the Mach number range $0.9 \leq M_\infty \leq 1.4$ at a Reynolds number of approximately 10^6. These values of sphere drag were found to be larger than the values derived from the experimental summary curves presented in Ref. 1. The change in sphere drag with Mach number near Mach 1, as well as with Reynolds number in excess of 10^5, is significant and care is required in establishing summary curves. On the basis of these more recent measurements and those contained in Refs. 2 and 3, the summary curves presented in Ref. 1 have been reevaluated. A plot of the revised values of sphere drag for $5 \times 10^2 \leq Re_\infty \leq 10^6$ and $0.1 \leq M_\infty \leq 1.75$ is presented in Fig. 1. The difference between the previous[1] and present values of sphere drag coefficient at $M_\infty = 0.955$ (Fig. 1) is representative of the changes that have been made, in the Mach number range of 0.8 to 1.5. Sphere drag coefficient is shown to increase with increasing Reynolds number for $10^5 \leq Re_\infty \leq 10^6$ for Mach numbers ranging from 0.9 to 1.75 (Fig. 1).

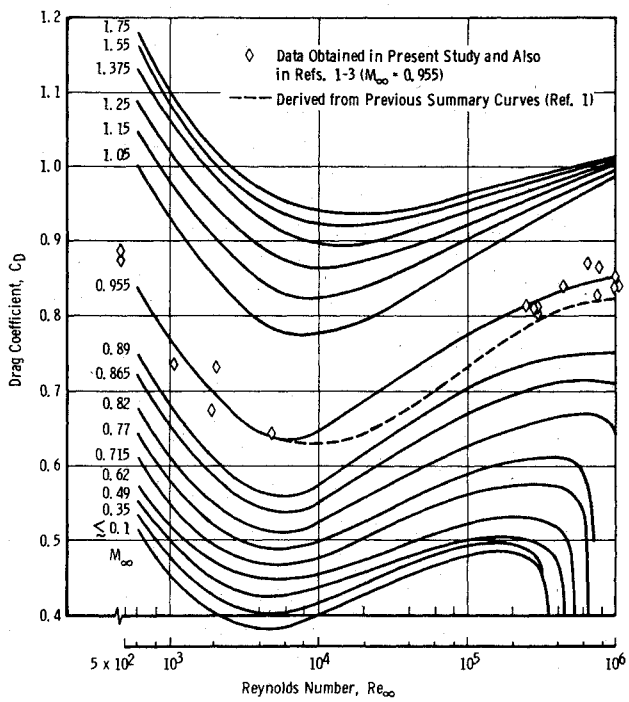

Fig. 1 Sphere drag coefficient variation with Mach and Reynolds number.

Received May 13, 1976. The research reported herein was conducted by the Arnold Engineering Development Center and sponsored by Air Force Cambridge Research Laboratories. Research results were obtained by personnel of ARO, Inc., contract operator of the Arnold Engineering Development Center (AEDC), Air Force Systems Command (AFSC), Arnold Air Force Station, Tennessee.

Index categories: Subsonic and Transonic Flow; Supersonic and Hypersonic Flow.

*Senior Research Engineer, Aerodynamics Projects Branch, von Karman Gas Dynamics Facility. Associate Fellow AIAA.

†Supervisor, 4T Projects Branch, Propulsion Wind Tunnel Facility. Member AIAA.

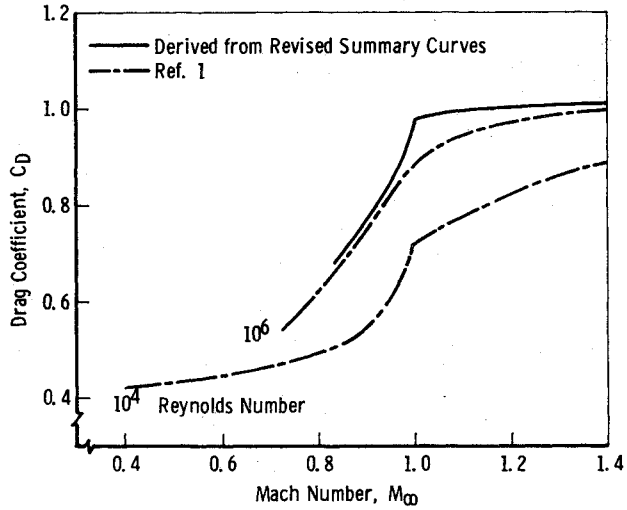

Fig. 2 Revised analysis of sphere drag in the transonic regime.

The variation of the revised values of C_D with M_∞ for $Re_\infty = 10^6$ are compared with the earlier values of Ref. 1 in Fig. 2. These revised values show a stronger dependence of C_D with M_∞ for $0.955 \leq M_\infty < 1.0$ than the $Re_\infty = 10^6$ values presented in Ref. 1.

References

[1] Bailey, A. B. and Hiatt, J., "Sphere Drag Coefficients for a Broad Range of Mach and Reynolds Numbers," *AIAA Journal*, Vol. 10, Nov. 1972, pp. 1436-1440.

[2] Short, B. J., "Dynamic Flight Behavior of a Ballasted Sphere at Mach Numbers from 0.4 to 14.5," NASA TN D-4198, Oct. 1967.

[3] Stilp, A., "Stromungsuntersuchungen an Kugeln mit transonischen und supersonischen Geschwindigkeiten in Luft und Frigen-Luftgemischen," Ernst-Mach-Institut, Freiburg/Br. Bericht Nr. 10/65.

Distribution Functions for Statistical Analysis of Monodisperse Composite Solid Propellant Combustion

Robert L. Glick*
Thiokol Corporation, Huntsville, Ala.

IN Ref. 1 a statistical basis for describing additive free composite propellant combustion was derived from continuity considerations. In this approach all states of all oxidizer particles populating the burning surface are incorporated into a rate defining expression through suitable distribution functions. These functions define the fraction of oxidizer particle/fuel surface pairs possessing planar surface areas ϵ_{ox} and ϵ_f such that (Nomenclature is the same as that of Ref. 1).

$$d^2N = NF_{ox}F_f d\epsilon_{ox} d\epsilon_f \tag{1}$$

In Ref. 1 the distribution functions F_{ox} and F_f were not related to propellant formulation and oxidizer variables. The

Received July 6, 1976. Research Sponsored by the Air Force Office of Scientific Research (AFSC), United States Air Force, under Contract F44620-74-C-0080. The United States Government is authorized to reproduce and distribute reprints for governmental purposes notwithstanding any copyright notation hereon.

Index categories: Combustion in Heterogeneous Media; Solid and Hybrid Rocket Engines.

*Principal Engineer, Advanced Design and Analysis Section. Member AIAA.

objective of this Note is to show how these functions are related to propellant formulation variables for propellants with monodisperse, spherical oxidizer.

In this analysis the propellant is assumed to be homogeneous and isotropic above a suitable length scale and oxidizer particles are assumed to be randomly arranged. In addition, the burning surface's topography is assumed to be, at most, a fuel plane with either convex and/or concave oxidizer surfaces.† Since a physiochemical combustion model is required to determine concavity or convexity of deflagrating oxidizer surfaces, attention is directed herein at the planar projection of oxidizer particle/fuel surface intersections. The aforementioned propellant structural assumptions are based on complete mixing of ingredients and the combustion model devised by Beckstread, Derr, and Price.[3]

With attention directed at planar intersections in a propellant that is homogeneous and isotropic above some length scale the distribution functions sought are identical to those for intersections exposed by a planar cut through the solid propellant. Since the volume fraction of oxidizer particles in the propellant is $\zeta = (\pi D_0^3/6)N_v$, the number of particles per unit volume is‡

$$N_v = 6\zeta/(\pi D_0^3) \tag{2}$$

Referring to Fig. 1, let the center of gravity (CG) denote the location of the sphere. Clearly, all particles intersecting S_p with $0 \le X \le \ell$ must have their CG's in the volume indicated. Therefore, the number of intersections with S_p for which $0 \le X \le \ell$ is

$$N_\ell = \ell N_v \tag{3}$$

Consequently, the total number of intersections with S_p is

$$N = 6\zeta/\pi D_0^2) \tag{4}$$

and the number of intersections for which $\ell \le X \le \ell + d\ell$ is

$$dN_\ell = 6\zeta d\ell/(\pi D_0^3) \tag{5}$$

Equation (5) shows that all latitudes of intersections are equally probable.§ Since $S_{p,ox}/S_p = \zeta = \bar{\epsilon}_{ox}N$, the areal mean planar intersection area for oxidizer particles is $\bar{\epsilon}_{ox} = \pi D_0^2/6$. Therefore, the areal mean diameter of all intersections

$$\bar{D}_{ox} = \sqrt{2/3}D_0 \tag{6}$$

Equations (4) and (6) agree with results employed by Ref. 3.

Since $dN/d\ell = NF_\ell = N/D_0$ and $dN/d\epsilon_{ox} = NF_{ox}$

$$F_{ox} = F_\ell(d\ell/d\epsilon_{ox}) \tag{7}$$

Referring to Fig. 1 and applying the Pythagorean theorem to triangle *abc* yields with some manipulation $\ell = D_0[1 \pm \sqrt{1-4\epsilon_{ox}/(\pi D_0^2)}]/2$. Differentiation gives

$$d\ell/d\epsilon_{ox} = \pm 1/[\pi D_0\sqrt{1-4\epsilon_{ox}/(\pi D_0)^2}] \tag{8}$$

Examination shows that ϵ_{ox} is doubly degenerate because neither northern nor southern hemisphere intersections can be distinguished solely from ϵ_{ox}. Consequently, $d\ell/d\epsilon_{ox}$ must be counted twice and since $F_{ox} \ge 0$, the positive value employed.

†This surface structure will be termed quasiplanar.

‡D = diameter of oxidizer particles.

§In Ref. 2 F_{ox} was computed for monodisperse spheres under the assumption (erroneous) that all ϵ_{ox} were equally probable.

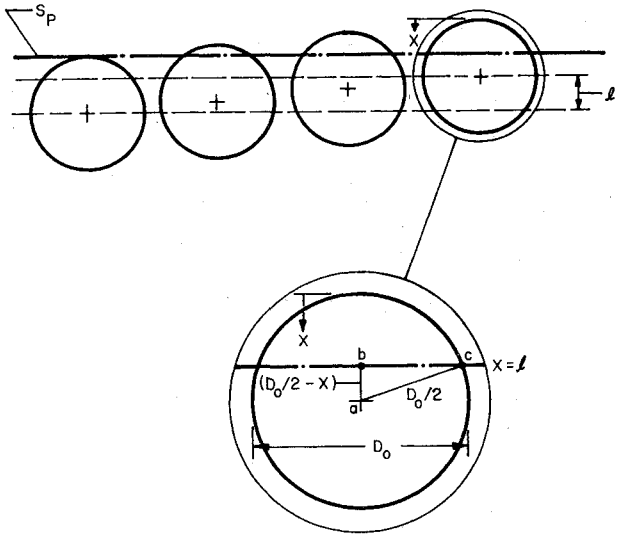

Fig. 1 Intersection geometry.

Therefore,

$$F_{ox} = 2/[\pi D_0^2\sqrt{1-4\epsilon_{ox}/(\pi D_0^2)}] \tag{9}$$

Equation (9) shows that F_{ox} is unbounded for equatorial intersections.

In the computation of the fuel distribution function there is no characteristic dimension. Consequently, the constraints on F_f are as follows

(I) All ϵ_f are equally probable

(II) $$\int_{\epsilon_f}^{\infty} F_f d\epsilon_f = 1 \tag{10}$$

(III) $$\int_{\epsilon_f}^{\infty} \epsilon_f F_f d\epsilon_f = \bar{\epsilon}_f \tag{11}$$

The second constraint arises because $\oint dN = N$; the third constraint arises because the fraction of the planar surface S_p that is fuel is $1-\zeta$. Since attention is focused on oxidizer particle/fuel surface pairs, the number of unit fuel surfaces is given by Eq. (4). Therefore, since $\bar{\epsilon}_f N = (1-\zeta)$

$$\bar{\epsilon}_f = (1-\zeta)\pi D_0^2/(6\zeta) \tag{12}$$

Comparison of constraints I-III with the basic constraints involved with the statistical mechanics of ideal gases (identify ϵ_f with particle energy)[4] shows they are equivalent. Consequently, the general form of the distribution function is the Boltzmann factor or

$$F_f = \exp(-\alpha)\exp(-\beta\epsilon_f) \tag{13}$$

where α and β are constants to be determined. Employing Eqs. (10)-(12) to evaluate α and β yields

$$F_f = \exp[-(\epsilon_f - \epsilon_f')/(\bar{\epsilon}_f - \epsilon_f')]/(\bar{\epsilon}_f - \epsilon_f') \tag{14}$$

Exact determination of ϵ_f' is complicated by the intricate central void geometry associated with the densest packing possible (rhombohedral unit cell[5]). Consequently, an estimate is offered herein. The smallest subcell in the unit cell is tetrahedral[5] so that a representative cross section is the area circumscribed by three equidiameter circles with centers at the apexes of an equilateral triangle. Therefore,

$$\epsilon_f' \sim D_0^2(2\sqrt{3}-\pi)/8 \tag{15}$$

Since F_{ox} is unbounded for equitorial intersections, ϵ_{ox} is degenerate, and all states are to be counted, the formulation proposed in Ref. 1 is inconsistent and should be revised. The length $0 \le \ell \le D_0$ defines the time from initial oxidizer particle exposure at the burning surface. Therefore, it uniquely defines all states. Consequently, replacing $F_{ox} d\epsilon_{ox}$ with $F_{ox,\ell}\, d\ell$¶ eliminates the aforementioned inconsistencies. This yields

$$\bar{m}_{ox} = N \int_0^{D_0} F_{ox,\ell} \epsilon_{ox} \int_{\epsilon_f}^{\infty} m_{ox} F_f d\epsilon_f d\ell \tag{16}$$

Equation (16) should replace Eq. (7) of Ref. 1. Extension of monodisperse distribution functions to polydisperse situations is treated in Ref. 2.

References

[1]Glick, R.L., "On Statistical Analysis of Composite Solid Propellant Combustion," *AIAA Journal,* Vol. 12. Mar. 1974, pp. 384-385.

[2]Glick, R.L., "Statistical Analysis of Non-Metallized Composite Solid Propellant Combustion," CPIA Publication 243, Vol. I, Dec. 1973, pp. 157-184.

[3]Beckstead, M.W., Derr, R.L., and Price, C.F., "A Model of Solid Propellant Combustion Based on Multiple Flames," *AIAA Journal,* Vol. 8, Dec. 1970, pp. 2200-2207.

[4]Dole, M., *Introduction to Statistical Thermodynamics,* Prentice-Hall, Inc., Englewood Cliffs, N.J., 1954, pp. 48-60.

[5]Dallavalle, J.M., Micromeritics, Pitman Publishing Company, New York, 1948, pp. 123-143.

¶As noted previously, $F_{ox,\ell} = 1/D_0$ for monodisperse situations.

Free-Interface Methods of Substructure Coupling for Dynamic Analysis

Roy R. Craig Jr.* and Ching-Jone Chang†
The University of Texas, Austin, Tex.

Introduction

SUBSTRUCTURE coupling methods have been developed in order to reduce the number of coordinates in a dynamic analysis of a complex structure, to permit analysis and design of different portions of a structure to proceed independently, and to permit testing of various portions of a structure to be done independently. References 1 and 2 survey most of the currently available methods with Ref. 2 providing numerical comparisons of the accuracy of eigenvalues obtained by a number of the methods. Substructure coupling methods can be classified as fixed-interface methods, free-interface methods, or hybrid methods, depending upon whether the mode shapes used to define substructure coordinates are obtained with the interface coordinates fixed, free, or a combination of the two. As noted by Benfield, et al.[2] the fixed-interface methods have been found to produce the best accuracy, while the free-interface methods of Hou and Goldman produced the poorest accuracy.

Although accuracy, or rate of convergence, is an important criterion to be used in selecting a substructure coupling method, two other important criteria are: substructure independence and test compatibility. None of the methods surveyed in Ref. 2 satisfies all three of the aforementioned criteria.

Several authors have suggested augmenting substructure normal modes in order to improve the convergence of free-interface methods.[3-6] In the present Note a substructure coupling method employing free-interface substructure normal modes supplemented by "reduced flexibility" will be presented. The basic ideas for representing the substructures are contained in the works of MacNeal[4] and Rubin.[6] The purpose of the present Note is to present a discussion of substructure coupling based on the improved substructure model and to present numerical results comparing the present method, which will be referred to as MacNeal's method, with Hou's method. To simplify presentation of the method here, the substructure equations are developed first for constrained substructures. Then the equations representing substructures with rigid-body modes are presented. Finally, the equations for coupling of substructures are developed, and examples are given.

Substructure Equations

Since the primary concern of this Note is to describe a substructure coupling method for use in calculating system modes and frequencies, only the equations of undamped vibration will be considered. For a given substructure, these may be written in the form

$$\begin{bmatrix} m_{ii} & m_{ij} \\ m_{ji} & m_{jj} \end{bmatrix} \begin{Bmatrix} \ddot{x}_i \\ \ddot{x}_j \end{Bmatrix} + \begin{bmatrix} k_{ii} & k_{ij} \\ k_{ji} & k_{jj} \end{bmatrix} \begin{Bmatrix} x_i \\ x_j \end{Bmatrix} = \begin{Bmatrix} 0 \\ f_j \end{Bmatrix} \tag{1}$$

where x_j is the set of junction (interface) coordinates, x_i is the set of interior coordinates, and f_j contains the forces transmitted to the substructure through junction coordinates. The free-interface modes are determined by the eigenvalue equation

$$[k - \lambda_\alpha^2 m]\, \phi_\alpha = 0 \tag{2}$$

The modes will be assumed to be normalized so that

$$\phi_\alpha^T\, m\, \phi_\alpha = 1, \qquad \phi_\alpha^T\, k\, \phi_\alpha = \lambda_\alpha^2 \tag{3}$$

and collected to form a modal matrix Φ.

A coordinate transformation relating physical coordinates, x, to modal coordinates p is given by

$$x = \Phi\, p \equiv \Phi_k\, p_k + \Phi_a\, p_a \tag{4}$$

where $\Phi_k\, p_k$ is the contribution of modes which are kept. The contribution $\Phi_a\, p_a$ will be replaced by an approximation.

When Eq. (4) is substituted into Eq. (1) there results a set of n equations of the form

$$\ddot{p}_\alpha + \lambda_\alpha^2\, p_\alpha = \phi_{j\alpha}^T\, f_j \tag{5}$$

If harmonic motion is assumed, i.e., $p = \bar{p} \cos\omega t$, etc., Eqs. (4) and (5) may be combined to give

$$\bar{x} = \sum_{\alpha=1}^{n} \phi_\alpha \left(\frac{\phi_{j\alpha}^T \bar{f}_j}{\lambda_\alpha^2 - \omega^2} \right) \doteq \sum_{\alpha=1}^{n_k} \phi_\alpha \left(\frac{\phi_{j\alpha}^T \bar{f}_j}{\lambda_\alpha^2 - \omega^2} \right) + \sum_{\alpha=n_k+1}^{n} \phi_\alpha \left(\frac{\phi_{j\alpha}^T \bar{f}_j}{\lambda_\alpha^2} \right) \tag{6}$$

The last series represents the "residual flexibility" of modes not explicitly kept. This can be obtained by subtracting from the flexibility matrix, $G = k^{-1}$, the contribution due to kept modes. Then Eq. (6) may be written as

$$\bar{x} = \Phi_k\, \bar{p}_k + G^a \bar{f} \tag{7}$$

Received Nov. 20, 1975; revision received Aug. 3, 1976. This work was supported by NASA Grant NSG 1001.

Index categories: Structural Dynamic Analysis; Aircraft Vibration; LV/M Dynamics, Uncontrolled.

*Associate Professor, Aerospace Engineering and Engineering Mechanics. Member AIAA.

†Graduate Student, Engineering Mechanics.